Efficient and accurate approach to modeling the microstructure and defect properties of $LaCoO_3$

J. Buckeridge,[*] F. H. Taylor, and C. R. A. Catlow

University College London, Kathleen Lonsdale Materials Chemistry, Department of Chemistry, 20 Gordon Street, London WC1H 0AJ, United Kingdom

(Received 22 January 2016; revised manuscript received 14 March 2016; published 14 April 2016)

Complex perovskite oxides are promising materials for cathode layers in solid oxide fuel cells. Such materials have intricate electronic, magnetic, and crystalline structures that prove challenging to model accurately. We analyze a wide range of standard density functional theory approaches to modeling a highly promising system, the perovskite $LaCoO_3$, focusing on optimizing the Hubbard U parameter to treat the self-interaction of the B-site cation's d states, in order to determine the most appropriate method to study defect formation and the effect of spin on local structure. By calculating structural and electronic properties for different magnetic states we determine that $U = 4$ eV for Co in $LaCoO_3$ agrees best with available experiments. We demonstrate that the generalized gradient approximation (PBEsol+U) is most appropriate for studying structure versus spin state, while the local density approximation (LDA+U) is most appropriate for determining accurate energetics for defect properties.

DOI: 10.1103/PhysRevB.93.155123

I. INTRODUCTION

Solid oxide fuel cells (SOFCs) work by using catalytic processes to oxidize a variety of fuels at the anode while reducing oxygen on the cathode side, balanced by ion transport through the cell, thus generating electrical power with water as the waste product when H_2 is used as fuel [1]. They are a promising clean energy resource, but, due to the chemical processes involved, high temperatures are required for efficient operation [2–6]. For next-generation SOFCs, cathode layers that can conduct both ions and electrons at intermediate temperatures (∼500–750 °C), while remaining stable and compatible with the other layers in the cell, are required [7–14]. One of the most promising materials for such cathode layers is the $LaCoO_3$-based system $La_{1-x}Sr_xFe_{1-y}Co_yO_3$ (LSCF) [15–21]. Finding the optimum doping concentrations for efficient fuel cell operation is, however, challenging, and input from computational modeling of the material properties in order to help formulate design improvements is crucial [22].

Many computational techniques have been employed to study different aspects of SOFCs, from mesoscopic models [23–25] to interatomic potential-based methods [26–31] and *ab initio* calculations [32–37]. To understand the key properties of LSCF, such as defect formation, ionic conductivity, mechanism of electronic conductivity, magnetic and electronic structure, and surface catalysis, requires an accurate but computationally tractable approach [22,38–43]. A fundamental requirement of such an approach is a sufficiently accurate description of the parent compound $LaCoO_3$.

At low temperatures, the perovskite $LaCoO_3$ stabilizes in the rhombohedral phase ($R\bar{3}c$; no. 167) [44–46]. As the temperature T is varied, an interesting magnetic effect is observed. At low T (below ∼50 K) $LaCoO_3$ is a diamagnetic insulator [47]. As T is increased above 50 K, a pronounced spin-state transition occurs, where the system becomes a paramagnetic semiconductor, with another transition possibly occurring at $T > 500$ K, where the system becomes metallic [47–49]. Associated with the spin transitions are variations in the local structure and splittings in optical phonon modes, possibly indicating a Jahn-Teller distortion [50–54]. The nature of the spin transition has been extensively studied experimentally and computationally [55–58], focusing on the d orbitals of the octahedrally coordinated Co ions, which are split by the crystal field. Initial proposals of a low spin (LS)–to–intermediate spin (IS) transition, possibly followed by a transition to high spin (HS) [48,59–63], have been superseded by more complicated scenarios involving different HS-LS orderings and possible defect-related effects to explain the experimental results [64–70]. Theoretical approaches applied include density functional theory (DFT) [71], using the local density approximation including a Hubbard U parameter (LDA+U) [60,72–75], dynamical mean-field theory [69,76], and higher-level quantum chemical approaches [61,77–80]. Despite the sophistication of the methods applied, which become more computationally intense as the complexity is increased, the nature of the spin-state transition remains a topic of debate [49,70,76,81–85].

To study defect properties, surface structure, and catalysis, the most common approaches have been DFT (including Hubbard U) [86–90] and interatomic force-field methods [26,27,91–93]. Such methods have been successful in modeling oxygen vacancy formation, ion migration, surface defect formation, and oxygen reduction, but their application has not concerned the effect of local structure variations on macroscopic magnetic properties.

In this paper, we analyze simple DFT approaches to modeling the structural, magnetic, and electronic properties of $LaCoO_3$, in order to determine the optimum method to be used in studying the defect and catalytic properties of the material, as well as the magnetic effects on the local structure. Our concern is to find the best method that is both accurate and computationally tractable. We find that, for defect studies, LDA+U is most advantageous, while for local structure and magnetism the generalized gradient approximation with a Hubbard U parameter (GGA+U) is the best of those surveyed. We find that a value of $U = 4$ eV is suitable in both cases. We demonstrate the applicability of our approaches by studying

[*]j.buckeridge@ucl.ac.uk

2469-9950/2016/93(15)/155123(8)

oxygen vacancy formation in the case of LDA+U and studying phonon mode splitting and local structure modification as the spin state varies in the case of GGA+U. Our results serve as a guide to future computational studies of the spin and defect properties of $LaCoO_3$.

The remainder of the paper is structured as follows. In Sec. II we describe the DFT approaches used; in Sec. III we present our results, and in Sec. IV we summarize the main points of our study.

II. CALCULATIONS

We have used DFT to calculate the structural, electronic, and magnetic properties of $LaCoO_3$ using a range of density functionals. All our DFT calculations were carried out using the VASP code [94–97], utilizing the projector augmented wave (PAW) method [98] to model core and valence electron interactions (using the "regular" PAW pseudopotential for O). The valence configurations used were La ($5s^25p^66s^25d^1$), Co ($4s^23d^7$), and O ($2s^22p^4$). To account for exchange and correlation, we have compared the LDA functional, the Perdew-Burke-Ernzerhof (PBE) GGA functional [99], and the PBE functional corrected for solids (PBEsol) [100]. Moreover, the effect of adding a Hubbard U parameter (LDA+U, PBE+U, PBEsol+U) has been investigated, using the rotationally invariant approach of Dudarev *et al.* [101]. As PBEsol was developed in order to reproduce lattice parameters more accurately than PBE [100], one would expect structural properties improved over those found using other GGA approaches [86–88,102,103] (but less accurate cohesive energies). Furthermore, PBEsol is known to model interatomic forces well, resulting in accurate phonon frequencies [36,104,105]. Hybrid functionals, where a fraction of the Hartree-Fock exact exchange is included [106–108], were tested but we do not report any results here, as we found that, as well as being prohibitively intensive computationally for larger systems, they represented the Co d states and material band gap in an erroneous manner, a result known from previous studies [109–111] on similar systems. (We have included a comparison of our calculated structural properties using hybrid DFT with those of Gryaznov *et al.* [112]; see [125].)

To avoid the problem of Pulay stress, the ion coordinates in the primitive rhombohedral cell (10 atoms) and the cell shape were optimized at constant volume for a series of different volumes, without enforcing symmetry constraints, and the resulting data fitted to the Murnaghan equation of state to determine the lowest energy structure. For IS and HS configurations, relaxations were performed using the pseudocubic expansion of the primitive cell (40 atoms), which allows symmetry-breaking Jahn-Teller distortions to occur if favorable. The two cells are shown in Fig. 1. The plane-wave cutoff energy used was 650 eV and Brillouin-zone sampling was performed, employing Gaussian smearing with a smearing width of 0.05 eV, on an $8\times8\times8$ Monkhorst-Pack [113] k-point mesh for the primitive cell and a $4\times4\times4$ k-point mesh for the pseudocubic cell, which provided convergence of up to 10^{-4} eV in the total energy. Geometry optimization was deemed to be converged when the interatomic forces were less than 10^{-2} eV/Å. For defect calculations, a $2\times2\times2$ expansion of the pseudocubic cell, i.e., a 320-atom supercell, was used, with k-point sampling performed at the Γ on a $2\times2\times2$ mesh.

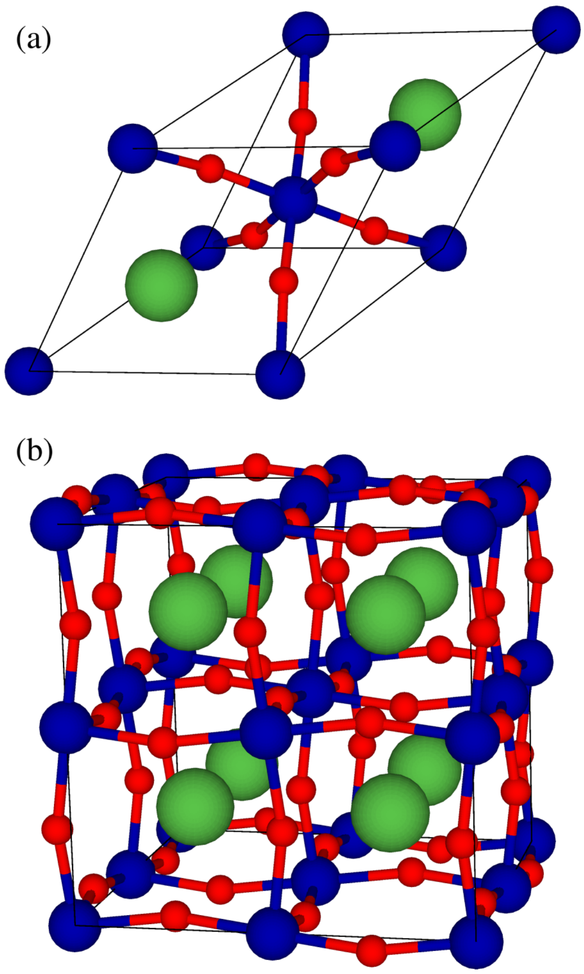

FIG. 1. Unit cells of $LaCoO_3$ used in this work. (a) The 10-atom primitive rhombohedral cell. (b) The 40-atom pseudocubic expansion of the primitive cell. Where necessary, periodically repeated atoms are shown for clarity. La ions are represented by large green spheres; Co ions, by intermediate-sized blue spheres; and O ions, by smaller red spheres.

With this supercell the minimum distance between periodic images of point defects is 14.95 Å.

Phonon frequencies at the Γ point were determined using the frozen phonon approach, where the dynamical matrix is derived by displacing atoms from their equilibrium positions and calculating the resulting forces, thus giving the force constants. Atomic displacements of 0.01 Å were used and the convergence criterion for the self-consistent field iterative procedure was 10^{-7} eV. These force calculations were performed using the pseudocubic cell, the geometry of which had been relaxed so that the interatomic forces were less than 10^{-4} eV/Å, in order to determine accurate phonon frequencies. The dynamical matrix was diagonalized and the eigenvectors analyzed using the postprocessing program PHONOPY [114].

The formation energy of a neutral oxygen vacancy, $E_f[V_O^\times]$ (where we use the standard Kröger-Vink [115] notation), assuming thermodynamic equilibrium, was determined from the equation

$$E_f[V_O^\times] = E_{\rm tot}[V_O^\times] - E_{\rm tot}[{\rm bulk}] + \tfrac{1}{2}\mu_{O_2}, \qquad (1)$$

TABLE I. Calculated rhombohedral lattice parameter (a) and angle (θ), determined using LDA, PBE, and PBEsol and compared with the low-temperature neutron diffraction measurements from Ref. [44].

	a (Å)	θ (deg)
Experiment	5.3416	60.99
LDA	5.2447	61.34
PBE	5.3613	61.20
PBEsol	5.2887	61.12

where E_{tot}[bulk] is the total energy of the pure $LaCoO_3$ bulk supercell, $E_{tot}[V_O^\times]$ is the total energy of the supercell containing a $V_O^\times$, and μ_{O_2} is the chemical potential of molecular oxygen. μ_{O_2} has been determined using the standard approach in supercell DFT calculations [116–119]. We assume thermodynamical equilibrium with a reservoir of oxygen gas under oxygen-rich conditions, so that μ_{O_2} is the energy of an O_2 molecule in the ground state (a triplet), i.e. excluding thermal contributions to the chemical potential.

III. RESULTS

We first discuss our calculated lattice parameter (a) and rhombohedral angle (θ) of the ground-state system using different density functionals, presented in Table I and Fig. 2. As our simulations are at the athermal limit, we compare our results with the low temperature (4 K) neutron diffraction measurements of Thornton *et al.* [44]. We find that the GGA and GGA+U functionals give values in good agreement with the experimental results (with differences of less than 1%), while LDA and LDA+U underestimate the parameters by ~2%. This underestimation is a well-known feature of the LDA [120].

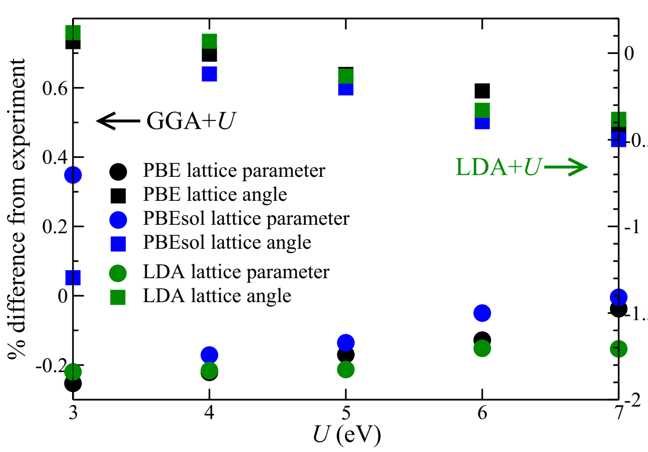

FIG. 2. Percentage difference between the low-temperature experimental [44] and the calculated rhombohedral lattice parameters (circles) and angles (squares), determined using the LDA+U (shown in green symbols), PBE+U (black symbols), and PBEsol +U (blue symbols), shown as a function of U. The scale on the left ordinate axis corresponds to GGA+U, while that on the right corresponds to LDA+U).

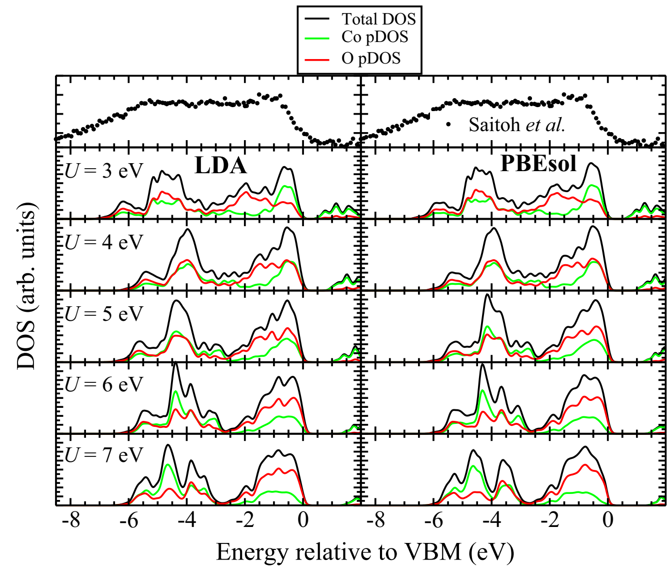

FIG. 3. Calculated density of states (DOS) (black lines) and partial DOS (pDOS) (Co pDOS, green lines; O pDOS, red lines) of $LaCoO_3$ determined using LDA+U and PBEsol+U, for different values of U. The energy scale is with respect to the valence-band maximum (VBM). For comparison the x-ray photoemission results of Saitoh *et al.* [61] are shown (black symbols).

We have calculated the electronic density of states (DOS) of $LaCoO_3$ (in the LS configuration) using different density functionals and present our results in Fig. 3, in comparison with the x-ray photoemission measurements of the upper valence band from Ref. [61]. We summarize the calculated band gaps (LS state) in Table II, including $U = 4$ eV cases as representative examples of our DFT+U results (see [125]). The energy gap was experimentally determined to be 0.6 eV [121] and 0.9 eV [59] using photoemission techniques and to be 0.1–1.1 eV using optical conductivity measurements [122–124]. We find that the LDA and GGA result in a metallic system, as expected due to the well-known self-interaction error and resulting band-gap underestimation that are a feature of these functionals. Adding a Hubbard U parameter allows one to open a gap, which may be tuned by varying U (although one can derive a U parameter from first principles, as done in Refs. [75] and [86]). From Fig. 3, it

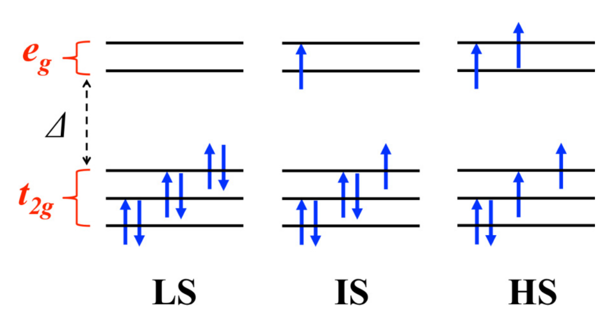

FIG. 4. Schematic of the idealized spin states on the octahedrally coordinated Co cations in $LaCoO_3$: low spin (LS), intermediate spin (IS), and high spin (HS). The crystal field splits the d states in energy (Δ), into e_g and t_{2g} orbitals. Upward-pointing arrows represent spin-up electrons; downward-pointing arrows, spin-down electrons.

TABLE II. The energy band gap (in eV) and ground-state spin configuration of $LaCoO_3$ as determined using different density functionals and compared with experimental results. "Metal" indicates zero gap. For brevity the $U = 4$ eV cases are included as representative of the DFT+U functionals (see [125] for an extension of this table). In each case the band gap is calculated for the LS state (see text for the definitions of the acronyms used for spin states).

	Experiment	LDA	PBE	PBEsol	LDA+U	PBE+U	PBEsol+U
Band gap (eV)	0.6 [121], 0.9 [59], 0.1–1.1 [122–124]	Metal	Metal	Metal	0.888	0.953	1.023
Spin state	LS	LS	LS	LS	LS	IS-HS FM	IS-HS FM

is evident that varying U also varies the valence band width, indicating that there is a trade-off between these two properties, which must be balanced when choosing an appropriate U value.

In $LaCoO_3$, the Co cations are octahedrally coordinated with a formal oxidation state of 3+, meaning that the six d electrons can occupy the e_g and t_{2g} orbitals in the configurations shown in Fig. 4; that is, in LS, IS or HS states. Moreover, the spin states can have ferromagnetic (FM) or antiferromagnetic (AFM) ordering among the Co-centred octahedra in different combinations, while it is also possible that there is ordered mixing of the LS, IS, and HS states. Which configuration is most favorable can be determined by calculating and comparing the total energies of the different spin combinations. We have performed such calculations to determine the ground-state configuration for each density functional considered in this study. Our results are presented in Table II (and see [125]). We find that LDA, GGA, and LDA+U result in an LS ground-state configuration, which agrees with experiment, as our simulations are at the athermal limit and $LaCoO_3$ is a diamagnetic insulator at low T. PBE+U and PBEsol+U result in an interesting ordered HS-IS FM configuration as the ground state, a point to which we return below.

To summarize the results presented so far, among the density functionals studied: for structural properties GGA functionals give the most accurate results; for electronic properties LDA+U and GGA+U are most accurate; and for magnetic properties LDA, GGA, and LDA+U are most accurate. Unsurprisingly, no simple DFT approach can accurately reproduce all these properties of $LaCoO_3$. Nevertheless, progress can be made by using LDA+U and PBEsol+U, as we demonstrate below. With LDA+U, a well-reproduced electronic and magnetic structure is gained, at the expense of slightly underestimated structural parameters. For defect calculations and studies of surface catalysis, the reproduction of accurate energetics is required, while errors introduced by underestimated structural parameters should largely cancel, meaning that LDA+U will be a suitable functional for such studies. We note that this approach has been studied previously [86] but was deemed inappropriate for oxygen vacancy formation calculations due to the calculated energy being higher than that determined experimentally, a point to which we return below. We find that PBEsol+U reproduces the structural parameters in excellent agreement with experiment, while also providing accurate electronic energies (although, as shown in Fig. 2, PBE+U also results in accurate structural properties, using PBEsol is known to model interatomic forces well [36,104,105], which are key for phonon frequency calculations). The calculated magnetic structures, however, involve mixtures of LS, IS, and HS that are all close in energy (the ground state being ordered IS-HS FM). The different structures are shown in Fig. 5, where the standard notation to distinguish different types of AFM ordering (A-, C-, and G-AFM) is used.

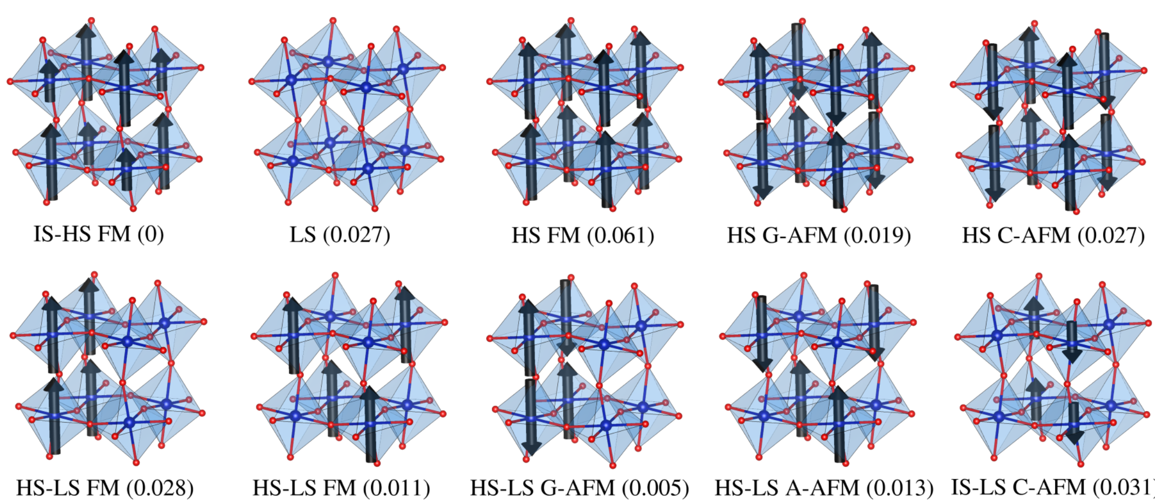

FIG. 5. Schematic of the different spin configurations that are close in energy when using the PBEsol+U functional. The different states are combinations of low-spin (LS), intermediate-spin (IS), and high-spin (HS) configurations with ferromagnetic (FM) or antiferromagnetic (AFM) ordering. AFM ordering can be of the A, C, or G type. Numbers in parentheses are the energy differences per atom (in eV) between the spin configuration shown and the ground state (IS-HS FM). Spins are indicated by black arrows, the relative length of which distinguishes HS and IS. Cocentered polyhedra are shown, with blue circles representing Co and red circles O. For clarity, La ions are not shown.

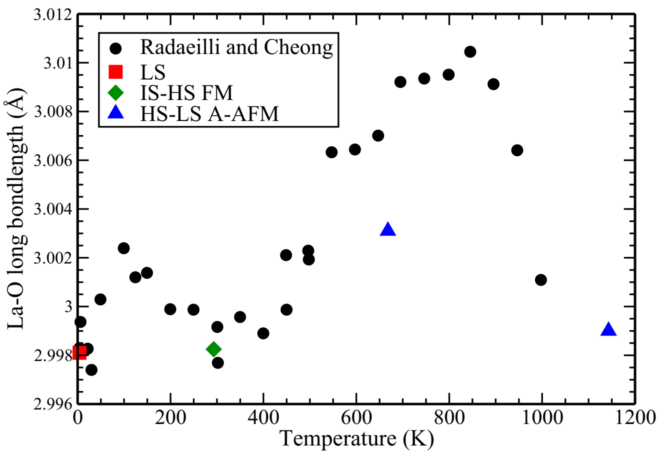

FIG. 6. La-O long bond length calculated at different volumes, corresponding to different temperatures, for the spin transition LS to IS-HS FM to HS-LS A-AFM (red square, green diamond, and blue triangles, respectively), compared with neutron diffraction measurements from Ref. [53] (black circles).

For the HS-LS mixtures we find either layers that alternate along the [100] direction or channels of HS (with FM or AFM ordering) along [$\bar{1}$01], while for the IS-LS mixture we find alternating channels along [001]. The ground-state IS-HS mix consists of alternating channels of each type along [$\bar{1}$01]. For pure HS, A-AFM could not be stabilized. The accurate structural properties, coupled with the different magnetic structures lying close in energy, mean that this functional may be useful in studying local structural changes vs spin state. Considering the electronic DOS shown in Fig. 3, we see that in varying the U parameter there is a trade-off between the energy band gap and the valence band width, as mentioned above. Setting $U = 4$ eV offers a good compromise in this trade-off for both LDA+U and PBEsol+U. This value agrees well with that used in previous studies [72,86]. We also note from Fig. 2 that a higher value of U would result in slightly more accurate structural properties. The improvement in the percentage difference from experiment between $U = 4$ and, e.g., $U = 7$, however, is less than 0.4%, which would not be a significant improvement given the drastically worse electronic properties obtained with $U = 7$. $U = 4$ offers the best compromise for electronic and structural properties (moreover, LS is no longer the ground state for LDA+U with $U = 7$ eV; see [125]).

To demonstrate the effectiveness of the PBEsol+U ($U = 4$ eV) density functional for studying the relationship between local structure and spin state, we have calculated, using the pseudocubic cell, the average La-O long bond length for the range of spin states shown in Fig. 5 at $T = 4, 273, 668$, and 1143 K in order to compare it with the neutron diffraction measurements of Radaelli and Cheong [53]. To simulate the different temperatures, we have fixed the lattice parameters to those determined experimentally by Thornton *et al.* [44] and allow the internal ionic coordinates to relax. If we fix the low-T bond length to that of Radeilli and Cheong [53] and analyze the differences in calculated bond length as the spin state is varied, we find that the transition from LS (at $T = 4$ K) to the IS-HS FM state (occurring between $T = 4$ and $T = 273$ K), followed by a transition to the HS-LS A-AFM state (at $T > 273$ K) reproduces the experimental trend well (see Fig. 6). Such a spin transition is consistent with experimental studies, where strong evidence of HS states is found after the initial transition at $T > 50$ K, rather than just IS spin states [64–70]. We can conclude, then, that the PBEsol+U approach can indeed be used successfully for such structural vs spin-state studies.

As a further example, we have calculated the zone-center phonon modes of $LaCoO_3$ in different spin configurations, using PBEsol+U, for comparison with the infrared (IR) measurements of Yamaguchi *et al.* [52]. At low T (and hence in the LS configuration), we calculate the IR stretching mode doublet to be 68 meV, in excellent agreement with experiment. Considering the transition to IS-HS FM ordering (see above), we find that the mode splits to 67 and 73 meV, again in excellent agreement with experiment [52]. (For the associated phonon density of states see [125].) This result further reinforces our conclusion that we can use this approach to study local structure vs spin state. Indeed, we find that, if we were to used LDA+U instead, the calculated low-T IR stretching mode doublet is 73 meV: an overestimation of $\sim$7%. As using LDA+U results in underestimated lattice parameters (see Fig. 2), this increase in the calculated frequency is unsurprising.

Using LDA+U, we have calculated the formation energy of an oxygen vacancy to be 3.44 eV, with AFM ordering of the neighboring reduced Co ions. Of these Co ions, the calculated magnetic moment $\mu = 1.6\mu_B$. This result is in good agreement with previous computational studies in the literature using a variety of theoretical approaches [33,86,87,92]. It is, however, significantly higher than the value of 2.2 eV determined experimentally [126], but given the low levels of nonstoichiometry observed in undoped $LaCoO_{3-\delta}$ ($\delta \leqslant 0.01$) [126], comparison with this value should take into account that vacancies on the surface may play a significant role in the reduction process. The surface vacancy formation energy has been determined to be lower than in the bulk by $\sim$1–2 eV [87,93] (this effect has also been determined in the related perovskite $LaMnO_3$ [40]). This result demonstrates that the LDA+U approach can be used for studies of defect properties of this material. If instead we employ the PBEsol+U functional, we immediately have the problem that the ground-state spin configuration of the defect-free system is not LS. When forming a defect, many spin configurations can be converged, and choosing the most appropriate one is difficult given that the original configuration is incorrect. Using the lowest total energy results, we calculate a formation energy of 6.14 eV, a value that is substantially higher than that determined using LDA+U and inconsistent with experimental results. Similar problems are expected when using PBE+U, as the ground-state spin configuration is also not LS in that case. These complications, which both lead to results that are probably not comparable with experiment and increase the computational load (due to the necessity of checking the many different possible configurations), lead us to conclude that GGA+U is considerably less favorable than LDA+U when studying defects.

IV. SUMMARY AND CONCLUSIONS

In summary, we have compared the results of calculated electronic, structural, and magnetic properties of $LaCoO_3$ using a range of standard density functionals in order to determine the optimum DFT approach for study of local distortions and defect formation. We found that no single DFT approach could model all these aspects accurately simultaneously but that two clear approaches, LDA+U and PBEsol+U, offered the most advantages for defect properties and structural studies vs spin states, respectively. We found that in both cases $U = 4$ eV gave results in good agreement with experiment. We demonstrated the applicability of these approaches by calculating the formation energy of an oxygen vacancy using LDA+U, finding excellent agreement with previous studies in the literature, and by determining the local structural variation and phonon mode splitting for different spin configurations, finding that the transition from LS to ordered HS-IS to HS resulted in a good agreement with experiment. Our results demonstrate that simple DFT methods can be used to study complex features of $LaCoO_3$.

ACKNOWLEDGMENTS

We are grateful to Prof. Saiful M. Islam for useful discussions. The authors acknowledge funding from EPSRC Grant No. EP/K016288/1. The authors also acknowledge the use of the UCL Legion High Performance Computing Facility (Legion@UCL) and associated support services, the IRIDIS cluster provided by the EPSRC-funded Centre for Innovation (Grant Nos. EP/K000144/1 and EP/K000136/1), and the ARCHER supercomputer through membership of the United Kingdom's HPC Materials Chemistry Consortium, which is funded by EPSRC Grant No. EP/L000202, in the completion of this work.

[1] S. C. Singhal and K. Kendall, in *High Temperature and Solid Oxide Fuel Cells*, edited by S. C. Singhal and K. Kendal (Elsevier Science, Amsterdam, 2003), pp. 1–22.
[2] S. C. Singhal, Solid State Ion. **135**, 305 (2000).
[3] R. M. Ormerod, Chem. Soc. Rev. **32**, 17 (2003).
[4] S. P. S. Badwal, Solid State Ion. **143**, 39 (2001).
[5] A. B. Stambouli and E. Traversa, Renew. Sustain. Energy Rev. **6**, 433 (2002).
[6] A. Lashtabeg and S. J. Skinner, J. Mater. Chem. **16**, 3161 (2006).
[7] B. C. H. Steele and A. Heinzel, Nature **414**, 345 (2001).
[8] A. Weber and E. Ivers-Tiffée, J. Power Sources **127**, 273 (2004).
[9] F. Tietz, Ionics **5**, 129 (1999).
[10] A. S. Aricò, P. Bruce, B. Scrosati, J.-M. Tarascon, and W. van Schalkwijk, Nat. Mater. **4**, 366 (2005).
[11] E. D. Wachsman and K. T. Lee, Science **334**, 935 (2011).
[12] Z. Shao and S. M. Haile, Nature **431**, 170 (2004).
[13] A. Tarancón, M. Burriel, J. Santiso, S. J. Skinner, and J. A. Kilner, J. Mater. Chem. **20**, 3799 (2010).
[14] J. M. Vohs and R. J. Gorte, Adv. Mater. **21**, 943 (2009).
[15] V. Dusastre and J. A. Kilner, Solid State Ion. **126**, 163 (1999).
[16] S. M. Haile, Acta Mater. **51**, 5981 (2003).
[17] A. Aguadero, L. Fawcett, S. Taub, R. Woolley, K.-T. Wu, N. Xu, J. A. Kilner, and S. J. Skinner, J. Mater. Sci. **47**, 3925 (2012).
[18] E. Ivers-Tiffée, A. Weber, and D. Herbstritt, J. Eur. Ceram. Soc. **21**, 1805 (2001).
[19] D. J. L. Brett, A. Atkinson, N. P. Brandon, and S. J. Skinner, Chem. Soc. Rev. **37**, 1568 (2008).
[20] H. Ullmann, N. Trofimenko, F. Tietz, D. Stöver, and A. Ahmad-Khanlou, Solid State Ion. **138**, 79 (2000).
[21] S. J. Skinner, Int. J. Inorg. Mater. **3**, 113 (2001).
[22] M. Liu, M. E. Lynch, K. Blinn, F. M. Alamgir, and Y. Choi, Mater. Today **14**, 534 (2011).
[23] M. Liu, J. Electrochem. Soc. **145**, 142 (1998).
[24] J. E. Saal, Ph.D. thesis, The Pennsylvania State University (2010).
[25] J. E. Saal, Y. Wang, S. Shang, and Z.-K. Liu, Inorg. Chem. **49**, 10291 (2010).
[26] M. S. Islam, M. Cherry, and C. R. A. Catlow, J. Solid State Chem. **124**, 230 (1996).
[27] M. Saiful Islam, J. Mater. Chem. **10**, 1027 (2000).
[28] S. M. Woodley, J. D. Gale, P. D. Battle, and C. R. A. Catlow, J. Chem. Phys. **119**, 9737 (2003).
[29] A. Jones and M. S. Islam, J. Phys. Chem. C **112**, 4455 (2008).
[30] A. Chroneos, B. Yildiz, A. Tarancon, D. Parfitt, and J. A. Kilner, Energy Environ. Sci. **4**, 2774 (2011).
[31] D. S. D. Gunn, N. L. Allan, and J. A. Purton, J. Mater. Chem. A **2**, 13407 (2014).
[32] A. B. Muñoz Garcìa, A. M. Ritzmann, M. Pavone, J. A. Keith, and E. A. Carter, Acc. Chem. Res. **47**, 3340 (2014).
[33] M. Pavone, A. M. Ritzmann, and E. A. Carter, Energy Environ. Sci. **4**, 4933 (2011).
[34] A. M. Ritzmann, A. B. Muñoz Garcìa, M. Pavone, J. A. Keith, and E. A. Carter, MRS Commun. **3**, 161 (2013).
[35] H.-T. Chen, P. Raghunath, and M. C. Lin, Langmuir **27**, 6787 (2011).
[36] J. Buckeridge, D. O. Scanlon, A. Walsh, C. R. A. Catlow, and A. A. Sokol, Phys. Rev. B **87**, 214304 (2013).
[37] X. Aparicio-Anglès, A. Roldan, and N. H. de Leeuw, Chem. Mater. **27**, 7910 (2015).
[38] J. Suntivich, H. A. Gasteiger, N. Yabuuchi, H. Nakanishi, J. B. Goodenough, and Y. Shao-Horn, Nature Chem. **3**, 546 (2011).
[39] Y. A. Mastrikov, R. Merkle, E. Heifets, E. A. Kotomin, and J. Maier, J. Phys. Chem. C **114**, 3017 (2010).
[40] S. Piskunov, T. Jacob, and E. Spohr, Phys. Rev. B **83**, 073402 (2011).
[41] D. Fuks, A. Weizman, and E. Kotomin, Phys. Status Solidi B **250**, 864 (2013).
[42] A. M. Ritzmann, A. B. Muñoz García, M. Pavone, J. A. Keith, and E. A. Carter, Chem. Mater. **25**, 3011 (2013).
[43] V. M. Tapilin, A. R. Cholach, and N. N. Bulgakov, J. Phys. Chem. Solids **71**, 1581 (2010).
[44] G. Thornton, B. Tofield, and A. Hewat, J. Solid State Chem. **61**, 301 (1986).
[45] V. Øygarden, H. L. Lein, and T. Grande, J. Solid State Chem. **192**, 246 (2012).
[46] C. Autret, J. Hejtmánek, K. KníŽek, M. MaryŠko, Z. Jirák, M. Dlouhá, and S. Vratislav, J. Phys.: Condens. Matter **17**, 1601 (2005).

[47] K. Asai, A. Yoneda, O. Yokokura, J. Tranquada, G. Shirane, and K. Kohn, J. Phys. Soc. Jpn. **67**, 290 (1998).
[48] C. Zobel, M. Kriener, D. Bruns, J. Baier, M. Grüninger, T. Lorenz, P. Reutler, and A. Revcolevschi, Phys. Rev. B **66**, 020402 (2002).
[49] A. Gulec and R. F. Klie, J. Appl. Phys. **116**, 233701 (2014).
[50] O. Haas, R. P. W. J. Struis, and J. M. McBreen, J. Solid State Chem. **177**, 1000 (2004).
[51] G. Maris, Y. Ren, V. Volotchaev, C. Zobel, T. Lorenz, and T. T. M. Palstra, Phys. Rev. B **67**, 224423 (2003).
[52] S. Yamaguchi, Y. Okimoto, and Y. Tokura, Phys. Rev. B **55**, R8666 (1997).
[53] P. G. Radaelli and S.-W. Cheong, Phys. Rev. B **66**, 094408 (2002).
[54] A. Ishikawa, J. Nohara, and S. Sugai, Phys. Rev. Lett. **93**, 136401 (2004).
[55] S. Stølen, F. Grønvold, H. Brinks, T. Atake, and H. Mori, Phys. Rev. B **55**, 14103 (1997).
[56] H. R. Aliabad, V. Hesam, I. Ahmad, and I. Khan, Physica B **410**, 112 (2013).
[57] S. K. Pandey, A. Kumar, S. Patil, V. R. R. Medicherla, R. S. Singh, K. Maiti, D. Prabhakaran, A. T. Boothroyd, and A. V. Pimpale, Phys. Rev. B **77**, 045123 (2008).
[58] W. T. Hong, M. Gadre, Y.-L. Lee, M. D. Biegalski, H. M. Christen, D. Morgan, and Y. Shao-Horn, J. Phys. Chem. Lett. **4**, 2493 (2013).
[59] M. Abbate, J. C. Fuggle, A. Fujimori, L. H. Tjeng, C. T. Chen, R. Potze, G. A. Sawatzky, H. Eisaki, and S. Uchida, Phys. Rev. B **47**, 16124 (1993).
[60] M. A. Korotin, S. Y. Ezhov, I. V. Solovyev, V. I. Anisimov, D. I. Khomskii, and G. A. Sawatzky, Phys. Rev. B **54**, 5309 (1996).
[61] T. Saitoh, T. Mizokawa, A. Fujimori, M. Abbate, Y. Takeda, and M. Takano, Phys. Rev. B **55**, 4257 (1997).
[62] D. Louca, J. L. Sarrao, J. D. Thompson, H. Röder, and G. H. Kwei, Phys. Rev. B **60**, 10378 (1999).
[63] Y. Kobayashi, T. S. Naing, M. Suzuki, M. Akimitsu, K. Asai, K. Yamada, J. Akimitsu, P. Manuel, J. M. Tranquada, and G. Shirane, Phys. Rev. B **72**, 174405 (2005).
[64] A. Podlesnyak, S. Streule, J. Mesot, M. Medarde, E. Pomjakushina, K. Conder, A. Tanaka, M. W. Haverkort, and D. I. Khomskii, Phys. Rev. Lett. **97**, 247208 (2006).
[65] M. W. Haverkort, Z. Hu, J. C. Cezar, T. Burnus, H. Hartmann, M. Reuther, C. Zobel, T. Lorenz, A. Tanaka, N. B. Brookes, H. H. Hsieh, H.-J. Lin, C. T. Chen, and L. H. Tjeng, Phys. Rev. Lett. **97**, 176405 (2006).
[66] R. Schmidt, J. Wu, C. Leighton, and I. Terry, Phys. Rev. B **79**, 125105 (2009).
[67] S. Medling, Y. Lee, H. Zheng, J. F. Mitchell, J. W. Freeland, B. N. Harmon, and F. Bridges, Phys. Rev. Lett. **109**, 157204 (2012).
[68] S. Ovchinnikov, Y. Orlov, and V. Dudnikov, J. Magn. Magn. Mater. **324**, 3584 (2012).
[69] V. Křápek, P. Novák, J. Kuneš, D. Novoselov, D. M. Korotin, and V. I. Anisimov, Phys. Rev. B **86**, 195104 (2012).
[70] S. El-Khatib, D. Phelan, J. G. Barker, H. Zheng, J. F. Mitchell, and C. Leighton, Phys. Rev. B **92**, 060404 (2015).
[71] P. Ravindran, P. A. Korzhavyi, H. Fjellvåg, and A. Kjekshus, Phys. Rev. B **60**, 16423 (1999).
[72] M. Abbate, R. Potze, G. A. Sawatzky, and A. Fujimori, Phys. Rev. B **49**, 7210 (1994).
[73] M. Sahnoun, C. Daul, O. Haas, and A. Wokaun, J. Phys.: Condens. Matter **17**, 7995 (2005).
[74] A. Laref and S. J. Luo, J. Phys. Soc. Jpn. **79**, 064702 (2010).
[75] H. Hsu, K. Umemoto, M. Cococcioni, and R. Wentzcovitch, Phys. Rev. B **79**, 125124 (2009).
[76] M. Izquierdo, M. Karolak, C. Trabant, K. Holldack, A. Föhlisch, K. Kummer, D. Prabhakaran, A. T. Boothroyd, M. Spiwek, A. Belozerov, A. Poteryaev, A. Lichtenstein, and S. L. Molodtsov, Phys. Rev. B **90**, 235128 (2014).
[77] H. Takahashi, F. Munakata, and M. Yamanaka, Phys. Rev. B **57**, 15211 (1998).
[78] R. Eder, Phys. Rev. B **81**, 035101 (2010).
[79] L. Siurakshina, B. Paulus, V. Yushankhai, and E. Sivachenko, Eur. Phys. J. B **74**, 53 (2010).
[80] Y. Wang, Z. Wang, Z. Fang, and X. Dai, Phys. Rev. B **91**, 125139 (2015).
[81] A. M. Durand, D. P. Belanger, C. H. Booth, F. Ye, S. Chi, J. A. Fernandez-Baca, and M. Bhat, J. Phys.: Condens. Matter **25**, 382203 (2013).
[82] A. M. Durand, D. P. Belanger, T. J. Hamil, F. Ye, S. Chi, J. A. Fernandez-Baca, C. H. Booth, Y. Abdollahian, and M. Bhat, J. Phys.: Condens. Matter **27**, 176003 (2015).
[83] J.-H. Kwon, W. S. Choi, Y.-K. Kwon, R. Jung, J.-M. Zuo, H. N. Lee, and M. Kim, Chem. Mater. **26**, 2496 (2014).
[84] J. Fujioka, Y. Yamasaki, A. Doi, H. Nakao, R. Kumai, Y. Murakami, M. Nakamura, M. Kawasaki, T. Arima, and Y. Tokura, Phys. Rev. B **92**, 195115 (2015).
[85] D. P. Belanger, T. Keiber, F. Bridges, A. M. Durand, A. Mehta, H. Zheng, J. F. Mitchell, and V. Borzenets, J. Phys.: Condens. Matter **28**, 025602 (2016).
[86] A. M. Ritzmann, M. Pavone, A. B. Muñoz Garcìa, J. A. Keith, and E. A. Carter, J. Mater. Chem. A **2**, 8060 (2014).
[87] A. Kushima, S. Yip, and B. Yildiz, Phys. Rev. B **82**, 115435 (2010).
[88] J. W. Han and B. Yildiz, J. Mater. Chem. **21**, 18983 (2011).
[89] S. O. Choi, M. Penninger, C. H. Kim, W. F. Schneider, and L. T. Thompson, ACS Catal. **3**, 2719 (2013).
[90] X. Cheng, E. Fabbri, M. Nachtegaal, I. E. Castelli, M. E. Kazzi, R. Haumont, N. Marzari, and T. J. Schmidt, Chem. Mater. **27**, 7662 (2015).
[91] M. Cherry, M. S. Islam, and C. R. A. Catlow, J. Solid State Chem. **118**, 125 (1995).
[92] M. S. D. Read, M. Saiful Islam, G. W. Watson, F. King, and F. E. Hancock, J. Mater. Chem. **10**, 2298 (2000).
[93] S. Khan, R. J. Oldman, F. Cora, C. R. A. Catlow, S. A. French, and S. A. Axon, Phys. Chem. Chem. Phys. **8**, 5207 (2006).
[94] G. Kresse and J. Hafner, Phys. Rev. B **47**, 558 (1993).
[95] G. Kresse and J. Hafner, Phys. Rev. B **49**, 14251 (1994).
[96] G. Kresse and J. Furthmüller, Comput. Mater. Sci. **6**, 15 (1996).
[97] G. Kresse and J. Furthmüller, Phys. Rev. B **54**, 11169 (1996).
[98] P. E. Blöchl, Phys. Rev. B **50**, 17953 (1994).
[99] J. P. Perdew, K. Burke, and M. Ernzerhof, Phys. Rev. Lett. **77**, 3865 (1996).
[100] J. P. Perdew, A. Ruzsinszky, G. I. Csonka, O. A. Vydrov, G. E. Scuseria, L. A. Constantin, X. Zhou, and K. Burke, Phys. Rev. Lett. **100**, 136406 (2008).
[101] S. L. Dudarev, G. A. Botton, S. Y. Savrasov, C. J. Humphreys, and A. P. Sutton, Phys. Rev. B **57**, 1505 (1998).

[102] K. Knížek, Z. Jirák, J. Hejtmánek, and P. Novák, J. Phys.: Condens. Matter **18**, 3285 (2006).
[103] K. Knížek, Z. c. v. Jirák, J. c. v. Hejtmánek, P. Novák, and W. Ku, Phys. Rev. B **79**, 014430 (2009).
[104] J. M. Skelton, S. C. Parker, A. Togo, I. Tanaka, and A. Walsh, Phys. Rev. B **89**, 205203 (2014).
[105] J. Buckeridge, D. O. Scanlon, T. D. Veal, M. J. Ashwin, A. Walsh, and C. R. A. Catlow, Phys. Rev. B **89**, 014107 (2014).
[106] M. Ernzerhof and G. E. Scuseria, J. Chem. Phys. **110**, 5029 (1999).
[107] J. Heyd, G. E. Scuseria, and M. Ernzerhof, J. Chem. Phys. **118**, 8207 (2003).
[108] J. Heyd, G. E. Scuseria, and M. Ernzerhof, J. Chem. Phys. **124**, 219906 (2006).
[109] K. G. Godinho, J. J. Carey, B. J. Morgan, D. O. Scanlon, and G. W. Watson, J. Mater. Chem. **20**, 1086 (2010).
[110] D. O. Scanlon and G. W. Watson, Phys. Chem. Chem. Phys. **13**, 9667 (2011).
[111] D. O. Scanlon and G. W. Watson, J. Mater. Chem. **21**, 3655 (2011).
[112] D. Gryaznov, R. A. Evarestov, and J. Maier, Phys. Rev. B **82**, 224301 (2010).
[113] H. J. Monkhorst and J. D. Pack, Phys. Rev. B **13**, 5188 (1976).
[114] A. Togo, F. Oba, and I. Tanaka, Phys. Rev. B **78**, 134106 (2008).
[115] F. A. Kröger and H. J. Vink, in *Solid State Physics* (Academic Press, New York, 1956), Vol. 3, pp. 307–435.
[116] C. G. V. de Walle and J. Neugebauer, J. Appl. Phys. **95**, 3851 (2004).
[117] C. Persson, Y.-J. Zhao, S. Lany, and A. Zunger, Phys. Rev. B **72**, 035211 (2005).
[118] J. Buckeridge, D. O. Scanlon, A. Walsh, and C. R. A. Catlow, Comput. Phys. Commun. **185**, 330 (2014).
[119] D. O. Scanlon, J. Buckeridge, C. R. A. Catlow, and G. W. Watson, J. Mater. Chem. C **2**, 3429 (2014).
[120] A. van de Walle and G. Ceder, Phys. Rev. B **59**, 14992 (1999).
[121] A. Chainani, M. Mathew, and D. D. Sarma, Phys. Rev. B **46**, 9976 (1992).
[122] T. Arima, Y. Tokura, and J. B. Torrance, Phys. Rev. B **48**, 17006 (1993).
[123] Y. Tokura, Y. Okimoto, S. Yamaguchi, H. Taniguchi, T. Kimura, and H. Takagi, Phys. Rev. B **58**, R1699 (1998).
[124] A. R. Sarker, Int. J. Mater. Sci. Appl. **4**, 159 (2015).
[125] See Supplemental Material at http://link.aps.org/supplemental/10.1103/PhysRevB.93.155123 for further data.
[126] J. Mizusaki, Y. Mima, S. Yamauchi, K. Fueki, and H. Tagawa, J. Solid State Chem. **80**, 102 (1989).